

Self-Propelled Droplet Removal from Hydrophobic Fiber-Based Coalescers

Kungang Zhang,¹ Fangjie Liu,¹ Adam J. Williams,¹ Xiaopeng Qu,¹ James J. Feng,^{2,3} and Chuan-Hua Chen^{1,*}

¹*Department of Mechanical Engineering and Materials Science, Duke University, Durham, North Carolina 27708, USA*

²*Department of Mathematics, University of British Columbia, Vancouver, British Columbia, Canada V6T 1Z2*

³*Department of Chemical and Biological Engineering, University of British Columbia, Vancouver, British Columbia, Canada V6T 1Z3*

(Received 30 November 2014; revised manuscript received 2 July 2015; published 14 August 2015)

Fiber-based coalescers are widely used to accumulate droplets from aerosols and emulsions, where the accumulated droplets are typically removed by gravity or shear. This Letter reports self-propelled removal of drops from a hydrophobic fiber, where the surface energy released upon drop coalescence overcomes the drop-fiber adhesion, producing spontaneous departure that would not occur on a flat substrate of the same contact angle. The self-removal takes place above a threshold drop-to-fiber radius ratio, and the departure speed is close to the capillary-inertial velocity at large radius ratios.

DOI: 10.1103/PhysRevLett.115.074502

PACS numbers: 68.08.Bc, 47.55.dr

Fiber-based coalescers are often used to remove droplets from aerosols and emulsions with a variety of applications ranging from water purification and food processing to oil refinery and gas plants [1–5]. The role of fibrous coalescers is to accumulate fine droplets which will merge into larger ones through successive coalescences. When the accumulated droplets grow large enough, they are typically removed by hydrodynamic shear or gravitational draining [5]. The requirement of external forces leads to ineffective sedimentation and undesired clogging in fibrous coalescers [4–8]. In this Letter, we report a self-propelled mechanism to remove the accumulated droplets from hydrophobic fibers. This new mechanism is powered by surface energy released upon drop coalescence and is therefore independent of external forces. Our work is distinct from prior studies of drop coalescence on a fiber, where the merged drops stay attached to the fiber after coalescence [9–14]. The surface-energy-powered detachment is related to the self-propelled jumping observed on superhydrophobic substrates [15–18], as well as superlyophobic and Leidenfrost ones [19,20]. However, the self-propelled motion reported here occurs on a round hydrophobic fiber (with a Young's contact angle $\gtrsim 90^\circ$) instead of a flat superhydrophobic substrate (with an apparent contact angle $\gtrsim 150^\circ$ [21]), circumventing the requirement of surface roughness for superhydrophobicity. This finding contrasts the fact that coalescing drops typically do not jump away from flat hydrophobic surfaces. As shown below, the curvature of the fiber plays a critical role in this surprising observation.

The accumulation and self-removal of condensate drops are studied on teflon-coated copper fibers of constant radius (Fig. 1). The setup is sketched in Fig. S1(a) with experimental procedures detailed in the Supplemental Material [22]. The fiber is coated with a thin layer of teflon with advancing and receding contact angles of $\theta_A = 121 \pm 3^\circ$ and $\theta_R = 108 \pm 2^\circ$, respectively. The fiber is cooled below

the dew point to induce condensation of the water vapor from the ambient air. Similar to the breath figure on flat substrates [23–26], the condensation on the hydrophobic fiber starts from isolated nuclei, but the condensate drops quickly grow large enough to merge with each other. In Fig. 1(a), many of the tiny drops at 3.0 s are already results of prior coalescences. The drop coalescence falls into two categories: (i) Immobile coalescence where the merged drop stays attached to the fiber, as in Fig. 1(b); (ii) mobile coalescence that frequently results in self-propelled

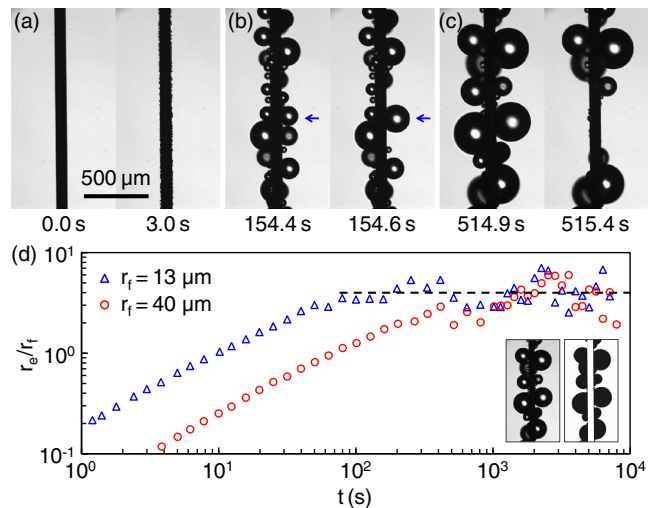


FIG. 1 (color online). Condensation on a teflon-coated fiber: (a) Initial period; (b) immobile coalescence of drops on the same side of the fiber; (c) mobile coalescence of drops on the opposite sides of the fiber; (d) the self-removal in (c) disrupts the growth of the effective thickness r_e with an asymptote $r_e/r_f \approx 4$ (dashed line) for two different fiber radii. The inset images illustrate the measurement of r_e using the projected area of condensate coverage while excluding the projected fiber area. The fiber radius $r_f = 40 \mu\text{m}$ in (a)–(c). Gravity points rightward. See also Videos S1 and S2 in the Supplemental Material [22].

detachment of the merged drop from the fiber, as in Fig. 1(c). Since the drop size is well below the capillary length, the self-removal in the last stage is independent of the gravitational orientation. The self-removal disrupts the accumulation of condensate drops on the fiber in Fig. 1(d). The average drop radius \bar{r}_d is indicated by an effective thickness measured as $r_e = A_e/(2l_f)$, where A_e is an effective area of the drop coverage defined in the inset of Fig. 1(d), and l_f is the fiber length. For two different fiber radii, the growth of the effective thickness approaches a limit of $r_e/r_f \approx 4$. As shown below, this limit is consistent with the existence of a critical radius ratio, $\bar{r}_d/r_f \approx \Gamma_{cr}$, above which drop coalescence leads to self-removal.

The self-removal process upon drop coalescence on smooth fibers has not been reported so far. A counterpart has been observed on roughened superhydrophobic surfaces with an apparent contact angle approaching 180° [15], on which two coalescing drops are known to jump out of plane in a self-propelled fashion. However, the smooth fiber used here only needs to be hydrophobic with a contact angle $\theta \gtrsim 90^\circ$ for the self-removal to occur. The curvature of the fiber cross section is essential (Fig. S2, [22]), as drops tend to stay attached upon coalescence on flat hydrophobic surfaces (Fig. S3, [22]). Even on round hydrophobic fibers, certain geometrical configurations are more conducive to the self-removal (Fig. S2, [22]). If the line connecting the centers of the coalescing drops is along the fiber axis as in Fig. 1(b), coalescence does not lead to self-removal from a teflon-coated fiber unless the drop-to-fiber radius ratio is above 8 or so (Fig. S4), well beyond the plateau regime in Fig. 1(d) with $r_e/r_f \approx 4$.

To explain the self-launching from hydrophobic fibers, we now turn to the simplified case of symmetric coalescence between two equally sized drops (Fig. 2). As a further restriction, the drops prior to coalescence are situated at the same axial location along the fiber, such that the line connecting the centers of mass is orthogonal to the fiber axis. Since the end view is particularly useful for

revealing the mechanism, we use conical fibers instead of uniform-radius ones from here on. The cones are produced with an apex angle of approximately 4° using procedures adapted from Ref. [27], and then coated with teflon. As shown in Fig. S1(b) [22], the thick conical base makes it possible to only fix and cool this stiff end, permitting the end view from the tip. The coalescence of two drops on the fiber is simultaneously visualized from both side and end views. A maneuvering probe is used to position the drops on the fiber and to induce the coalescence of two drops. Unless otherwise noted, the drop radii are nearly identical, each within 6% of the average drop radius (r_d). To minimize the interference, the tip of the maneuvering probe is much smaller than the local radius (r_f) of the conical fiber, measured at the point of drop coalescence. For further details, see Ref. [22].

A representative coalescence process between two equal drops on opposite sides of the fiber is shown in Fig. 2. The end view indicates a two-step process for the self-propelled launching of the merged drop. First, the fiber interferes with the coalescence process and breaks its top-bottom symmetry, leading to acceleration of the merged drop orthogonal to the fiber, until it is almost completely displaced to one side of the fiber (around 1.2 ms). Second, the inertia of the merged drop competes against the adhesion from the fiber, leading to necking of the liquid bridge between the merged drop and the fiber (1.8 ms) toward an eventual snap off (2.1 ms), at which point the detached drop is launched into the air with an initial velocity (v).

The essence of the two-step launching process in Fig. 2(a) is numerically reproduced in Fig. 3(a) with two-dimensional (2D) phase-field simulations following [28,29]. The drop coalescence process on the fiber is then compared to that on the substrate in Fig. 3(b). Despite its 2D nature [30], Fig. 3 is representative of all low-Ohnesorge-number cases with $Oh = \mu/\sqrt{\rho\sigma r_d} \lesssim 0.1$, where μ is the liquid viscosity, ρ is the liquid density, σ is the liquid-gas surface tension, and r_d is the initial radius

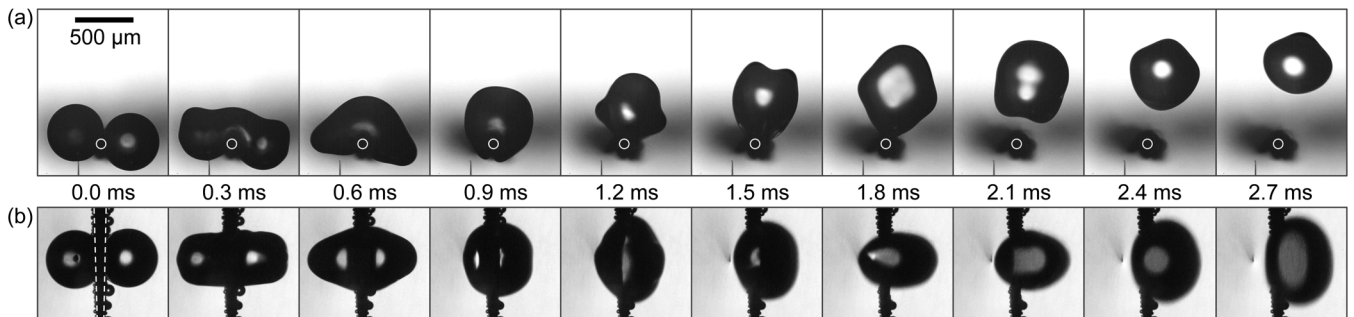


FIG. 2. Self-propelled departure process upon coalescence of symmetric drops, where the line connecting the initial drop centers are orthogonal to the fiber axis: (a) End view with the estimated location of the fiber denoted by a white circle; (b) side view with the conical fiber denoted by dashed lines. A second fiber visible in (a) is used as the maneuvering probe. Gravity points rightward in both (a) and (b). The average drop radius (r_d) is $249 \mu\text{m}$ and the fiber radius (r_f) is $46 \mu\text{m}$ ($r_d/r_f = 5.4$). See also Videos S3 and S4 in the Supplemental Material [22].

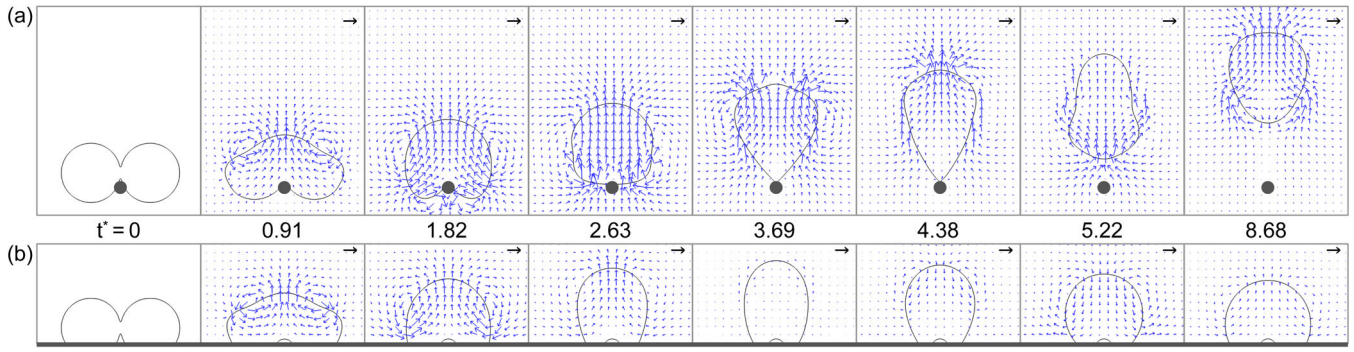


FIG. 3 (color online). Two-dimensional simulations with $Oh = 0.0126$ and $\theta = 120^\circ$: (a) On a round fiber with $r_d/r_f = 5$; (b) on a flat substrate. For coalescence between liquid cylinders [30], the self-launching occurs only on the fiber with a much smaller liquid-solid contact area. The unit vector corresponds to the capillary-inertial velocity u_{ci} , and the time is reduced by t_{ci} . The nondimensional time stamps (t^*) are chosen according to Fig. S5, [22]. See also Videos S5 and S6 in the Supplemental Material [22].

of the identical drops prior to coalescence. In such cases, the coalescence process is governed by the capillary-inertial velocity and time, $u_{ci} = \sqrt{\sigma/(\rho r_d)}$ and $t_{ci} = \sqrt{\rho r_d^3/\sigma}$.

In Fig. 3, self-launching takes place on the fiber, but not on the substrate with the same contact angle of 120° . On the substrate, the drop-substrate adhesion prohibits the self-launching so the merged drop merely oscillates back and forth. On the fiber, the liquid-solid contact area is greatly reduced and self-launching occurs. Although the initial coalescence processes are similar until $t^* = 1.82$, the merged drop starts to decelerate on the substrate beyond this point, but continues to accelerate on the fiber until $t^* = 2.63$ (see also Fig. S5). As a result, the merged drop attains a substantially larger forward momentum on the fiber compared to that on the substrate. Although the merged drop also starts to decelerate beyond $t^* = 2.63$, the adhesive force from the fiber is much smaller than that from the substrate, and the adhesion is overpowered by the substantial forward momentum. This overpowering leads to the departure from the fiber beyond $t^* = 4.38$ with a nondimensional launching velocity v^* .

Based on the two-step process in Fig. 2, the launching velocity (v) can be modeled through an energetic argument. For the merged drop to detach from the hydrophobic fiber with a translational kinetic energy, the released surface energy upon drop coalescence must overcome the adhesion between the drops and the fiber; therefore,

$$\begin{aligned} \rho r_d^3 v^2 &= c_1 \sigma r_d^2 - \hat{c}_2 (\sigma + \sigma_{SG} - \sigma_{SL}) r_d r_f \\ &= c_1 \sigma r_d^2 - c_2 \sigma r_d r_f. \end{aligned} \quad (1)$$

The prefactors c_1 and c_2 (\hat{c}_2) absorb the algebraic and geometrical factors and also implicitly account for some physical details: c_1 accounts for the partial energy conversion from surface to kinetic energy, noting that the efficiency is almost constant in a related process

[28]; $c_2 = \hat{c}_2(1 + \cos\theta)$ accounts for the static and dynamic factors in overcoming the work of adhesion, $\sigma + \sigma_{SG} - \sigma_{SL} = \sigma(1 + \cos\theta)$, where σ_{SG} and σ_{SL} are, respectively, the solid-gas and solid-liquid surface tensions. The Young's contact angle θ is fixed for a given combination of working fluid and fiber-coating material, provided that the hysteresis ($\Delta\theta = \theta_A - \theta_R$) is small. Note that the drop radius r_d appears in the adhesion term because the merged drop extends in the longitudinal direction before launching, which is apparent in the side view Fig. 2(b). The characteristic length of the longitudinal extension is r_d , which is larger than the fiber radius r_f for the self-launching system studied here.

Equation (1) applies to symmetric coalescences on hydrophobic fibers ($\theta \gtrsim 90^\circ$) with $\Delta\theta \ll \theta$ and $r_f < r_d$. From Eq. (1), the nondimensional self-launching velocity is

$$v^* = \frac{v}{u_{ci}} = \sqrt{c_1 - \frac{c_2}{r_d/r_f}} = v_\infty^* \sqrt{1 - \frac{\Gamma_{cr}}{\Gamma}}, \quad (2)$$

where $\Gamma = r_d/r_f$ is the drop-to-fiber radius ratio. The constants have been replaced by physically significant symbols: $c_1 = v_\infty^{*2}$, where v_∞^* denotes the reduced velocity at an infinitely large radius ratio: $c_2 = v_\infty^{*2} \Gamma_{cr}$, where Γ_{cr} denotes the critical radius ratio for the merged drop to detach from the fiber. Note that $v^{*2} = \rho v^2 r_d / \sigma$ is formally the same as the Weber number, for which v would be an externally imposed velocity. Rearranging Eq. (2),

$$v = v_\infty^* \sqrt{1 - \frac{\Gamma_{cr}}{\Gamma}} \sqrt{\frac{1}{\Gamma} \sqrt{\frac{\sigma}{\rho r_f}}} \leq \frac{v_\infty^*}{2\sqrt{\Gamma_{cr}}} \sqrt{\frac{\sigma}{\rho r_f}}. \quad (3)$$

The maximum dimensional velocity is achieved when the radius ratio satisfies $\Gamma = 2\Gamma_{cr}$.

The simple model in Eqs. (1)–(3) is indeed supported by Fig. 4 with symmetric coalescences on teflon-coated fibers. As suggested by Eq. (2), the constants in the semiempirical model are extracted from a linear fit to the measured v^{*2}

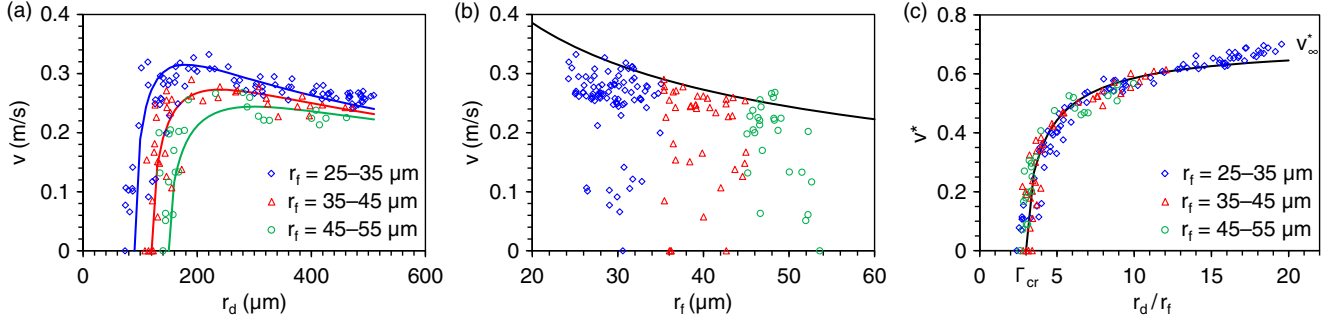


FIG. 4 (color online). The measured launching velocities plotted against the theoretical model: (a) The velocity orthogonal to the fiber (v) as a function of drop radius (r_d). The experimental data are grouped into three ranges of drop radii. The theoretical curves are plotted according to Eq. (1), with $r_f = 30, 40,$ and $50 \mu\text{m}$ from top to bottom. (b) The measured velocities are bounded by the maximum predicted by Eq. (3), which is a function of the fiber radius (r_f). (c) The data collapse onto a nondimensional curve $v^*(\Gamma)$ given by Eq. (2), where $v^* = \sqrt{\rho v^2 r_d / \sigma}$ and $\Gamma = r_d / r_f$. For water drops on teflon fibers, $v_\infty^* = 0.7$ and $\Gamma_{\text{cr}} = 3$ for all theoretical curves. Note that data points are excluded in the occasional case of the coalesced drop “wrapping” around the fiber prior to departure (Fig. S6, [22]).

versus $1/\Gamma$, yielding $v_\infty^* = 0.7 \pm 0.05$ and $\Gamma_{\text{cr}} = 3 \pm 0.5$. In Fig. 4(a), the measured velocity is plotted against the drop radius, and the data can be grouped by fiber radii to theoretical curves predicted by Eq. (1). In Fig. 4(b), the dimensional velocity is now plotted against the fiber radius, and the velocity is roughly bounded by the maximum velocity given by Eq. (3) with $\Gamma = 2\Gamma_{\text{cr}}$. Most significantly, in Fig. 4(c), all measurements collapse on to a single curve in accordance with Eq. (2).

The energetic argument in Eq. (1) can be extended to model asymmetric coalescences between a larger drop (r_d) and a smaller one (r'_d), despite the complex rotational motion arising from the asymmetry (Fig. S7, [22]). For the asymmetric coalescence, the translational kinetic energy is dominated by the larger drop mass, while the surface energy variations are governed by the smaller drop radius [20]. Accordingly, Eq. (1) is modified to $\rho r_d^3 v^2 = c_1 \sigma r_d'^2 - c_2 \sigma r'_d r_f$. Indeed, asymmetric coalescences on teflon fibers roughly follow this modified equation with the same constants as the corresponding symmetric case (Fig. S8, [22]). The launching velocity scales as $(r'_d / r_d) u_{\text{ci}}$, while the critical condition for launching is governed by $r'_d / r_f > \Gamma_{\text{cr}}$.

A hydrophobic fiber with $\theta \gtrsim 90^\circ$ is needed for the self-propelled launching to occur. With similar r_d / r_f ratios, the self-launching does not occur on copper fibers coated with polystyrene ($\theta_A / \theta_R = 93^\circ / 68^\circ$, Fig. S9, [22]), but occurs on those coated with alkythiol ($110^\circ / 74^\circ$, Fig. S10, [22]) and teflon ($121^\circ / 108^\circ$, Fig. 2). For the alkythiol fiber with a larger adhesive force compared to the teflon fiber, the launching velocity is reduced (Fig. S11, [22]), and a residual drop is sometimes left behind after the main drop detaches from the fiber (Fig. S10, [22]).

Compared to the flat substrate in Fig. S2(c) [22], the highly curved fiber in Fig. S2(a) [22] enables self-launching from a moderately hydrophobic surface with a remarkably high energy conversion efficiency. The conversion efficiency from the released surface energy to

translational kinetic energy scales with v^{*2} [28]. On flat substrates with contact angles up to 180° , the efficiency is below 4% [20,28]. On round fibers with a contact angle of only 120° or so, the efficiency is already approaching 40% at large r_d / r_f (Fig. 4). The fiber gives rise to a higher efficiency not only by reducing the liquid-solid contact area, but also by intervening in the drop coalescence process at a much earlier stage. The fiber is positioned much closer than the substrate to the expanding liquid bridge, and therefore intervenes in the coalescence when the surface energy release is barely starting and significant oscillatory motion has not developed. With such an early intervention, the released energy is more effectively harnessed toward useful translational motion. For example, when the surface energy release is near a local maximum with a mostly rounded drop, the drop motion is predominantly translational on the fiber (around $t^* = 1.82$ in Fig. 3), and mainly oscillatory on the substrate (around $t^* = 1.88$ in Fig. 7 of Ref. [28]). The early intervention mechanism also partially explains why coalescence on the opposite sides of the fiber in Fig. S2(a) [22] is more conducive to self-launching compared to that on the same side in Fig. S2(b) [22].

Equipped with the insights from Figs. 2–4, we can now explain the self-removal phenomenon on the fibrous coalescers. The observation in Fig. 1 results from the coalescence of multiple drops, which is confirmed by high-speed imaging [31]. The self-removal usually involves at least two of these drops situated on opposite sides of the fiber axis, e.g., Fig. 1(c), so that the merged drop is launched by the self-propelled mechanism illustrated in Fig. 2. The average drop size in the self-removal regime is roughly $r_e \approx 4r_f$ for the teflon-coated fiber in Fig. 1(d), which is reasonable considering the critical condition of $r_d \approx 3r_f$ in Fig. 4(c) for the ideally situated drops to launch upon coalescence.

The critical condition for self-removal can be exploited to control the average size of the droplets spontaneously

removed from fibrous coalescers. For a small drop impacting a fiber of a given radius r_f , a critical drop radius exists below which the capillary adhesion from the fiber overcomes the drop's inertia toward a drop capture [32]. When the captured drops grow large enough on the fiber with $r_d/r_f \gtrsim \Gamma_{cr}$, the surface energy released upon coalescence creates enough drop inertia to overcome the adhesion from the fiber, and the merged drop self-launches away.

In summary, we have reported a self-propelled removal mechanism for droplets accumulated on fibrous coalescers. The self-removal mechanism is powered by surface energy released upon drop coalescence and is therefore independent of external forces. The round fiber enables the self-propelled process to occur on smooth hydrophobic surfaces, even though a similar process does not occur on flat hydrophobic substrates. Although we have focused on liquid coalescence in the gas phase, our preliminary results indicate that the self-propelled mechanism can also work if the coalescence is in another liquid phase, as long as the viscosities of both liquids are moderate [31]. In addition to coalescers, the self-removal process on hydrophobic fibers may find applications in other fields such as water harvesting [13] and dropwise condensation [33].

This work was supported by the National Science Foundation (CBET-12-36373). A. J. W. was supported by the Pratt Fellows Program at Duke University. J. J. F. was supported by the Natural Sciences and Engineering Research Council of Canada. The authors gratefully acknowledge Hadi Mehrabian and Thomas Witelski for helpful discussions. C. H. C. thanks Gregory and Jolanta Watson for kindling his interest in fibrous structures.

*chuanhua.chen@duke.edu

- [1] R. E. Treybal, *Liquid Extraction* (McGraw-Hill, New York, 1963).
- [2] A. Burkholz, *Droplet Separation* (VCH, New York, 1989).
- [3] T. Wines, *Hydrocarb. Process.* **79**, 89 (2000).
- [4] T. Frising, C. Noik, and C. Dalmazzone, *J. Dispersion Sci. Technol.* **27**, 1035 (2006).
- [5] B. Tilley and T. Witelski, Modeling industrial coalescers: droplet dynamics, *Proceedings of the 28th Annual Workshop on Mathematical Problems in Industry, Newark, DE (2012)*, <http://www.maths-in-industry.org/miis/613/1/pall2012.pdf>.
- [6] N. I. Kolev, *Exp. Therm. Fluid. Sci.* **6**, 211 (1993).
- [7] P. Contal, J. Simao, D. Thomas, T. Frising, S. Callé, J. Appert-Collin, and D. Bémer, *J. Aerosol Sci.* **35**, 263 (2004).
- [8] K.-C. Park, S. S. Chhatre, S. Srinivasan, R. E. Cohen, and G. H. McKinley, *Langmuir* **29**, 13269 (2013).
- [9] J. F. Bitten, *J. Colloid Interface Sci.* **33**, 265 (1970).
- [10] A. Steyer, P. Guenoun, D. Beysens, D. Fritter, and C. Knobler, *Europhys. Lett.* **12**, 211 (1990).
- [11] B. J. Briscoe, K. P. Galvin, P. F. Luckham, and A. M. Saeid, *Colloids Surf.* **56**, 301 (1991).
- [12] A. L. Yarin, G. G. Chase, W. Liu, S. V. Doiphode, and D. H. Reneker, *AIChE J.* **52**, 217 (2006).
- [13] Y. Zheng, H. Bai, Z. Huang, X. Tian, F.-Q. Nie, Y. Zhao, J. Zhai, and L. Jiang, *Nature (London)* **463**, 640 (2010).
- [14] S. Agarwal, V. von Arnim, T. Stegmaier, H. Planck, and A. Agarwal, *Sep. Purif. Tech.* **107**, 19 (2013).
- [15] J. B. Boreyko and C.-H. Chen, *Phys. Rev. Lett.* **103**, 184501 (2009).
- [16] C. Dietz, K. Rykaczewski, A. G. Fedorov, and Y. Joshi, *Appl. Phys. Lett.* **97**, 033104 (2010).
- [17] N. Miljkovic, R. Enright, Y. Nam, K. Lopez, N. Dou, J. Sack, and E. N. Wang, *Nano Lett.* **13**, 179 (2013).
- [18] K. Rykaczewski, A. T. Paxson, S. Anand, X. Chen, Z. Wang, and K. K. Varanasi, *Langmuir* **29**, 881 (2013).
- [19] M. Kollera and U. Griggull, *Heat Mass Transfer* **2**, 31 (1969).
- [20] F. Liu, G. Ghigliotti, J. J. Feng, and C.-H. Chen, *J. Fluid Mech.* **752**, 22 (2014).
- [21] D. Quéré, *Rep. Prog. Phys.* **68**, 2495 (2005).
- [22] See Supplemental Material at <http://link.aps.org/supplemental/10.1103/PhysRevLett.115.074502> for experimental procedures, additional data, and supplemental videos.
- [23] D. Beysens, *C.R. Phys.* **7**, 1082 (2006).
- [24] D. Beysens and C. M. Knobler, *Phys. Rev. Lett.* **57**, 1433 (1986).
- [25] J. L. Viovy, D. Beysens, and C. M. Knobler, *Phys. Rev. A* **37**, 4965 (1988).
- [26] M. Sokuler, G. Auernhammer, C. Liu, E. Bonaccorso, and H. Butt, *Europhys. Lett.* **89**, 36004 (2010).
- [27] É. Lorenceau and D. Quéré, *J. Fluid Mech.* **510**, 29 (2004).
- [28] F. Liu, G. Ghigliotti, J. J. Feng, and C.-H. Chen, *J. Fluid Mech.* **752**, 39 (2014).
- [29] H. Mehrabian and J. J. Feng, *J. Fluid Mech.* **752**, 670 (2014).
- [30] The two-dimensionality of the simulations has introduced some artifacts: the adhesion due to drop-fiber contact is unrealistically amplified in Fig. 3(a), and a pocket of air is artificially trapped between the drops and the substrate in Fig. 3(b).
- [31] K. Zhang, Master's Thesis, Duke University, 2014.
- [32] É. Lorenceau, C. Clanet, and D. Quéré, *J. Colloid Interface Sci.* **279**, 192 (2004).
- [33] X. Qu, J. B. Boreyko, F. Liu, R. L. Agapov, N. V. Lavrik, S. T. Retterer, J. J. Feng, C. P. Collier, and C.-H. Chen, *Appl. Phys. Lett.* **106**, 221601 (2015).